Single-Nanoparticle Electrochemistry through Immobilization and Collision

Todd J. Anderson and **Bo Zhang**[*]

Department of Chemistry, University of Washington, Seattle, Washington 98195, United States

Conspectus
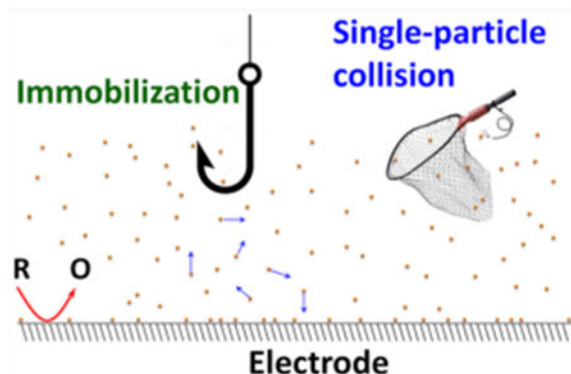
Metal nanoparticles are key electrode materials in a variety of electrochemical applications including basic electron-transfer study, electrochemical sensing, and electrochemical surface enhanced Raman spectroscopy (SERS). Metal nanoparticles have also been extensively applied to electrocatalytic processes in recent years due to their high catalytic activity and large surface areas. Because the catalytic activity of metal nanoparticle is often highly dependent on their size, shape, surface ligands, and so forth, methods for examining and better understanding the correlation between particle structure and function are of great utility in the development of more efficient catalytic systems. Despite considerable progress in this field, the understanding of the structure–activity relationships remains challenging in nanoparticle-based electrochemistry and electrocatalysis due to limitations associated with traditional ensemble measurements. One of the major issues is the ensemble averaging of the electrocatalytic response which occurs over a very large number of nanoparticles of various sizes and shapes. Additionally, the electrochemical response can also be greatly affected by properties of the ensemble itself, such as the particle spacing.

The ability to directly measure kinetics of electrochemical reactions at structurally well-characterized single nanoparticles opens up new possibilities in many important areas including nanoscale electrochemistry, electrochemical sensing, and nanoparticle electrocatalysis. When a macroscopic electrode is placed in a solution containing redox molecules and metal nanoparticles, random collision and adsorption of nanoparticles occurs at the electrode surface in addition to

[*]Corresponding Author: Phone: 206 543 1767. zhang@chem.washington.edu.

Notes: The authors declare no competing financial interest.

redox reactions when a suitable potential is present on the electrode. In a special case where particles are catalytically more active than the substrate, the faradaic signals can be greatly amplified on particle surfaces and a steady shift in the baseline current would be expected due to many particles adsorbing on the electrode.

Single particle events can be temporally resolved when an ultramicroelectrode (UME) is used as the recording electrode. The use of an UME not only reduces the collision frequency, but also greatly decreases baseline noise, thereby resulting in clear resolution of single collision events. Single particle collision has quickly grown into a popular electroanalytical technique in recent years. Alternatively, one can use nanoelectrodes to immobilize single nanoparticles so that they can be individually studied in electrochemistry and electrocatalysis. Nanoparticle immobilization also allows one to obtain detailed structural information on the same particles and offers enormous potential for developing more comprehensive understanding of the structure–function relationship in nanoparticle-based electrocatalysts. This Account summarizes recent electrochemical experiments of single metal nanoparticles which have been performed by our group using both of these schemes.

1. Introduction

Nanoparticles have received tremendous attention in recent decades due to their unique structure-dependent catalytic properties. For example, Ni and Pd nanoparticles show high activity for methanol oxidation on their {111} crystal facets.[1,2] Nanoparticle size[3–5] and surface ligands[6–9] also have clear effects on their catalytic activity. While these studies have made use of nanoparticle ensembles, averaging effects and possible overlap between the diffusion layers of separate particles can negatively impact the utility of electrochemical information gained from such measurements. Methods for examining individual nanoparticles are therefore highly desirable.

Our research toward understanding electrochemistry and electrocatalysis at single nanoparticles includes work with nanoparticle immobilization and collision. In the first method, a nanoparticle is isolated through attachment to the tip of a nanoelectrode followed by potential scanning to record single particle response; immobilization may be achieved via direct adsorption to an electrode surface,[10,11] electrodeposition,[12–14] or electrostatic interaction.[15,16] Nanoparticle collision involves the detection of an enhanced faradaic signal from single nanoparticles colliding on a microelectrode. Although this exact scheme was introduced by the Bard group,[17–21] a similar procedure was originally described by Lemay and co-workers in which nanoparticle collisions were detected via current inhibition.[22]

In the realm of nanoparticle immobilization, single Au particles were attached to chemically modified Pt or Au nanoelectrodes.[15,23] The resulting single nanoparticle electrodes (SNPEs) were then characterized via transmission electron microscopy (TEM), cyclic voltammetry, and underpotential deposition (UPD) of Cu. This method can be used to determine how the voltammetric response of a nanoparticle is related to size and shape. This scheme was also used to investigate the oxygen reduction reaction (ORR) in order to demonstrate single nanoparticle electrocatalysis.

Many exciting experiments involving nanoparticle collisions have been reported by the Bard group[24–27] and several others.[28–43] In our group, AgCl has been deposited onto a carbon fiber microelectrode (CFE) and used as a redox indicator for particle collision.[44] Additionally, we have employed fast-scan cyclic voltammetry (FSCV) in particle collision experiments.[45] The use of FSCV offers unique chemical resolution and the ability to extract kinetic parameters on single colliding nanoparticles.[46]

2. Single-Particle Immobilization

Single nanoparticle immobilization requires the use of nanoelectrodes whose dimensions are comparable to the particle size. To demonstrate this concept, individual Au nanoparticles have been attached to the tips of laser-pulled Pt nanoelectrodes. This approach has enabled the collection of faradaic responses from single nanoparticles.[15] A key step in this method is the fabrication and functionalization of nanoelectrodes approaching molecular dimensions.

Pt nanoelectrodes with tip radii approaching 2 nm were created in a laser puller.[47] Briefly, a Pt microwire was inserted and sealed in a piece of quartz capillary tubing. The microwire/quartz assembly was pulled into two nanowire tips followed by tip exposure. Au nanoelectrodes were also fabricated by etching the exposed Pt followed by Au deposition and polishing.[23] Nanoparticle immobilization was accomplished through the use of a molecular linker $(CH_3O)_3Si(CH_2)_3NH_2$ on the Pt surface or 1,6-hexanethiol on Au. Single-particle immobilization allows one to use electron microscopy to correlate nanoparticle structure with electrochemical response. Figure 1a shows a TEM image of a ~15 nm Au nanoparticle immobilized on an ~10 nm Pt nanoelectrode. The particle size can also be determined through Cu UPD.

Au SNPEs were also characterized with cyclic voltammetry prior to TEM or UPD analysis. The CVs of a bare Pt electrode with and without silane-modification, and after immobilizing an Au nanoparticle were recorded in $K_3Fe(CN)_6$ as shown in Figure 1b. Note the lower current exhibited by the silane-modified electrode relative to bare Pt which is due to the higher electron-transfer resistance of the silane monolayer. The larger signal of the Au SNPE is due to the larger nanoparticle size and the enhanced electron tunneling across the monolayer. An interesting negative shift is observed in the $E_{1/2}$ after silane modification, thereby indicating that an increase in the irreversibility accompanies this change.

The increasing current observed in Figure 1b indicates that the limiting current is dependent more on the size of the Au nanoparticle and less on the base electrode. The limiting current, i_d, at the Au nanoparticle can be estimated using the following equation which corresponds to a spherical electrode on a large surface

$$i_d = 4\pi(\ln 2)nFDC_b a \quad (1)$$

where F is the Faraday constant, D and C_b are the diffusion coefficient and bulk concentration of the redox molecule, respectively, n is the number of electrons transferred, and a is the nanoparticle radius.

In order to demonstrate the utility of these Au SNPEs in nanoparticle electrocatalysts, the voltammetric response of Au SNPEs in ORR was examined. The CVs in Figure 1c correspond to ORR on a bare Pt nanoelectrode and three Au nanoparticles of different sizes. Attachment of the Au nanoparticle results in a fast reduction wave with a half-wave potential of only −0.07 V and ORR current that is correlated to the particle size. These results indicate that the Au nanoparticles exhibits good ORR activity. Note also from Figure 1c that increasing steady-state currents and decreasing half-wave potential are associated with increasing nanoparticle size, an observation which indicates somewhat paradoxically that larger particles are more catalytically active. However, the validity of such a conclusion is rendered somewhat questionable when the effects of particle size on the rate of diffusion are taken into account. The effects of mass transport rate on $E_{1/2}$-values are discussed in greater detail in section 3.2 below.

In summary, single-particle immobilization is of great utility in the study of individual nanoparticles. The use of a nanoelectrode support opens up new opportunities to correlate electrochemical property with nanoparticle structure at a true single-nanoparticle level. This method may also enable one to study optical properties of individual nanoparticles under electrochemical control. However, this method has low throughput and exhibits challenges in nanoparticle imaging which need to be addressed in future studies.

3. Single-Nanoparticle Collision

The method of single-particle collision is an exciting alternative for examining the faradaic current response of large numbers of individual nanoparticles, albeit without obtaining detailed structural information. Collision and adsorption of nanoparticles and molecular species on an electrode are common processes in electrochemical systems. These processes can take place on a macroscopic electrode at exceedingly high frequencies, and are therefore challenging to individually resolve under normal conditions. A key factor in the resolution of single collision events is the use of an UME which allows one to greatly reduce the collision frequency.

When catalytically active nanoparticles come into contact with an inert UME in a solution of redox molecules (e.g., hydrazine), transient current increases may be observed due to enhanced catalytic activity on nanoparticle surfaces (see Figure 2). The current response of these collisions may adopt one of two general forms: a staircase pattern or a blip pattern. If the nanoparticles desorb or deactivate on a time scale that is relatively long compared to that of the experiment, the result is an amperometric curve which exhibits an increasing series of current plateaus (a "staircase" pattern). If particle desorption or deactivation is fast, a current response resembling a series of sharp spikes ("blips") may be observed.

3.1. AgCl Reduction as a Collision Indicator

Because redox molecules in solution can negatively affect the stability of the nanoparticles, a method which does not require the presence of such species is desirable. One such scheme involves the reduction of AgCl patches deposited on a CFE.[44] Because AgCl reduction on Ag is much faster than on carbon, Ag nanoparticles can be readily detected on an AgCl-modified CFE. This method used a square-shape voltage waveform to detect collision of Ag

nanoparticles. First, a + 400 mV potential vs Ag/AgCl was applied on the carbon to oxidize 80 nm Ag nanoparticles and to form patches of insulating AgCl. A reduction potential was subsequently applied on the same electrode in order to detect nanoparticle collisions when they catalyzed the reduction of AgCl back to Ag. Figure 3 shows detection traces at five reduction potentials. The low frequency indicates that a collision event may only be observed at or near the location of the deposited AgCl. The absence of detection spikes in the −600 mV trace may be attributed to the fact that all of the AgCl patches on the electrode were directly reduced on carbon. This process was also used to detect 4 nm Au nanoparticles. Thus, the use of AgCl on a CFE provides a general detection strategy for metal nanoparticles.

3.2. Single-Particle Collision by Fast-Scan Cyclic Voltammetry

Nanoparticle collision experiments are simple and can probe hundreds of particles in a few minutes. However, the actual chemical information obtained is limited because only a single peak current is recorded from each particle. In order to address this challenge, FSCV has been used to study Pt and Au nanoparticles in hydrazine.[45] In FSCV, the electrostatic potential on a CFE was continuously scanned at fast scan rates up to 1000 V/s, thereby allowing a series of CVs to be collected for each new particle adhering to the electrode surface.

Figure 4a displays an FSCV color plot of five collision events of Pt nanoparticles recorded at 400 V/s. Figure 4b and c displays the current–voltage trace at +0.1 V and a CV at 7.7 s, respectively. Note that the falling current subsequent to each spike in the current–time trace may be attributed to particle deactivation. Despite the rapid scan rate, the CV in Figure 4c nevertheless exhibits a sigmoidal shape arising from rapid diffusion and kinetic limitation.
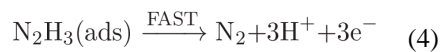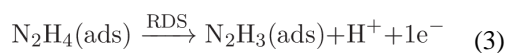
A unique feature of FSCV is the ability to obtain chemical resolution. An FSCV color plot displaying 11 collisions recorded in a mixed solution of Pt and Au nanoparticles is shown in Figure 5a, while Figure 5b shows three CVs collected for the 5th, 8th, and 11th nanoparticles. Due to their different catalytic activities, particles of differing compositions may be readily distinguished from one another via their CVs. The CV shown for the fifth collision (black trace) is therefore indicative of an Au particle, the eighth (blue trace) indicates Pt, and the 11th (red trace) indicates a dual Au–Pt particle.

FSCV can also be used to better explain the catalytic activity of single nanoparticles.[46] Onset potentials (E_{onset}) and half-wave potentials ($E_{1/2}$) were extracted from Pt and Au single-particle CVs in hydrazine. Surprisingly, all of the particles exhibited increasing E_{onset} and $E_{1/2}$ values with decreasing particle size. This trend is exemplified especially well in Figure 6 which displays plots of average $E_{1/2}$ and E_{onset} versus inverse particle radius for both Au and Pt nanoparticles. An explanation for these seemingly unexpected results lies in the faster mass transfer of reactants (hydrazine) on smaller nanoparticles. In order for the forward reaction rate (which is determined by the value of the forward rate constant, k_a) to match this increased rate of mass transfer, a larger potential must be applied, as is indicated by eq 2 below

$$k_\mathrm{a} = k^\circ \exp\left[(1-\alpha)\left(\frac{nF}{RT}\right)(E_\mathrm{app} - E^\circ)\right] \quad (2)$$

where k° is the standard electron transfer rate constant, α is the charge transfer coefficient, E_app is the applied potential, E° is the standard potential of hydrazine, R is the gas contact, T is absolute temperature, and other factors are previously defined. The increased positive shift exhibited on the 10 nm nanoparticles may be attributed to their cubic shape and larger polyacrylate ligands.

Due to these increased mass transfer effects, the relative electrocatalytic activity of single nanoparticles of different sizes may not be determined through simple comparisons of E_onset and $E_{1/2}$ values without also conducting appropriate kinetic analyses. One can model the diffusion and oxidation of hydrazine at the surface of a single nanoparticle using numerical simulation. Adsorbed hydrazine oxidation occurs according to an initial 1-e⁻ rate-determining step (RDS), after which three subsequent fast 1-e⁻ processes take place, as is shown below.

$$\mathrm{N_2H_4(ads)} \xrightarrow{\text{RDS}} \mathrm{N_2H_3(ads)} + \mathrm{H^+} + 1\mathrm{e^-} \quad (3)$$

$$\mathrm{N_2H_3(ads)} \xrightarrow{\text{FAST}} \mathrm{N_2} + 3\mathrm{H^+} + 3\mathrm{e^-} \quad (4)$$

Note that the overall rate of this reaction is determined by the forward rate constant, k_a, as defined in eq 2. The flux of hydrazine molecules to the surface of a nanoparticle may be expressed according to eq 5 below

$$j = -k^\circ \exp\left[(1-\alpha)\left(\frac{F}{RT}\right)(E_\mathrm{app} - E^\circ)\right]C_\mathrm{R} \quad (5)$$

where C_R is the hydrazine concentration at the electrode and all other parameters have been previously defined. Using this model, simulated CVs were generated and the values of α and k° were varied until the simulation matched the experimental CVs. Figure 7 shows overlay plots of simulated and experimental CVs and the corresponding α and k° values. Note that while there appears to be good correlation exhibited between the simulated and experimental data, the discrepancies observed for the larger nanoparticles may be attributed to nanoparticle geometry. This effect could result in surface roughness or the appearance of specific crystal faces which are better capable of accommodating preadsorption of hydrazine, thereby resulting in faster hydrazine oxidation during the anodic scan and explaining the peaks which are observed in the experimental CVs from panels (b) and (d) of

Figure 7. Particle deactivation may also contribute to these peaks, although the extent of such effects is not entirely clear.

The values of α and k° extracted from different sized Au and Pt nanoparticles are summarized in Table 1. One can see a very clear increasing trend in k° is exhibited as particle size decreases. It is also interesting to note that all of the Pt nanoparticles exhibit larger α-values than their Au counterparts. A possible explanation for this observation is that proton adsorption on Pt may block catalytic sites and hinder hydrazine oxidation. In contrast, Au exhibits a much lower proton affinity.

To summarize, FSCV is a powerful technique which not only provides unique chemical resolution, but also enables the estimation of kinetic parameters at single nanoparticles. This method therefore exhibits tremendous potential in future electrocatalytic studies at single nanoparticles. The temporal resolution of FSCV is slightly lower than amperometry due to the requirement for continuous voltage scan. However, FSCV can provide useful mechanistic information which can be difficult or impossible to obtain with other methods.

4. Conclusions and Future Work

Single-particle measurements hold great potential for better understanding nanoparticle electrocatalysis. TEM imaging, single-particle immobilization and collision are all powerful techniques for probing the structure–function relationships of metal nanoparticles while avoiding ensemble averaging. However, there are certain shortcomings which are specific to each technique. Single-particle immobilization provides an excellent balance between electrochemical information gained through voltammetry and structural information obtained via TEM. However, it is both challenging and exhibits low throughput at the current stage. Single-particle collision allows one to analyze hundreds of nanoparticles in a few minutes, albeit at the cost of obtaining only a single peak current at a given voltage for each colliding particle (analogous to a single point in a CV) with no structural information at all. Incorporation of FSCV into single-particle collision increases the amount of electrochemical information that may be obtained; the absence of structural information is still an issue, however. Single-particle collision coupled with in situ TEM and FSCV could therefore provide an exciting focus for future research. Such an amalgamation of techniques would enable the collection of both structural and electrochemical information through time-correlation of TEM images collected following individual collision events with the corresponding CVs.

Acknowledgments

References

1. Zhou M, Xiao P, Guo W, Deng J, Liu F, Zhang Y. Electrochemical Synthesis of Monodisperse Nickel with Predominant {111} Orientation and High Electro-Oxidation Activity for Methanol. J Electrochem Soc. 2014; 161:H133–H137.

2. Wang R, He H, Liu LC, Dai HX, Zhao Z. Shape-Dependent Catalytic Activity of Palladium Nanocrystals for the Oxidation of Carbon Monoxide. Catal Sci Technol. 2012; 2:575–580.

3. Tritsaris GA, Greeley J, Rossmeisl J, Norskov JK. Atomic-Scale Modeling of Particle Size Effects for the Oxygen Reduction Reaction on Pt. Catal Lett. 2011; 141:909–913.

4. Bergamaski K, Pinheiro ALN, Teixeira-Neto E, Nart FC. Nanoparticle Size Effects on Methanol Electrochemical Oxidation on Carbon Supported Platinum Catalysts. J Phys Chem B. 2006; 110:19271–19279. [PubMed: 17004779]

5. Ge X, Peng B, Ying X, Wang R, Liu X, Xiao F, Qiu S, Li J. In-Situ Transmission Electron Microscopy Observation of Particle Size Effect of Nanoscale Platinum Catalysts on the Formation of Fullerenelike Carbon Shells. Carbon. 2008; 46:1411–1416.

6. Que Y, Feng C, Zhang S, Huang X. Stability and Catalytic Activity of PEG-b-PS-Capped Gold Nanoparticles: A Matter of PS Chain Length. J Phys Chem C. 2015; 119:1960–1970.

7. Janani S, Stevenson P, Veerappan A. Activity of Catalytic Silver Nanoparticles Modulated by Capping Agent Hydrophobicity. Colloids Surf B. 2014; 117:528–533.

8. Liu W, Wang H. Influence of Surface Capping on Oxygen Reduction Catalysis: A Case Study of 1.7 nm Pt Nanoparticles. Surf Sci. 2016; 648:120–125.

9. Gavia DJ, Shon YS. Controlling Surface Ligand Density and Core Size of Alkanethiolate-Capped Pd Nanoparticles and Their Effects on Catalysis. Langmuir. 2012; 28:14502–14508. [PubMed: 22924990]

10. Kim J, Kim BK, Cho SK, Bard AJ. Tunneling Ultramicroelectrode: Nanoelectrodes and Nanoparticle Collisions. J Am Chem Soc. 2014; 136:8173–8176. [PubMed: 24857267]

11. Hill CM, Kim J, Bard AJ. Electrochemistry at a Metal Nanoparticle on a Tunneling Film: A Steady-State Model of Current Densities at a Tunneling Ultramicroelectrode. J Am Chem Soc. 2015; 137:11321–11326. [PubMed: 26280667]

12. Chen S, Kucernak A. Electrodeposition of Platinum on Nanometer-Sized Carbon Electrodes. J Phys Chem B. 2003; 107:8392–8402.

13. Chen S, Kucernak A. Electrocatalysis under Conditions of High Mass Transport Rate: Oxygen Reduction on Single Submicrometer-Sized Pt Particles Supported on Carbon. J Phys Chem B. 2004; 108:3262–3276.

14. Clausmeyer J, Masa J, Ventosa E, Ohl D, Schuhmann W. Nanoelectrodes Reveal the Electrochemistry of Single Nickelhydroxide Nanoparticles. Chem Commun. 2016; 52:2408–2411.

15. Li Y, Cox JT, Zhang B. Electrochemical Responses and Electrocatalysis at Single Au Nanoparticles. J Am Chem Soc. 2010; 132:3047–3054. [PubMed: 20148588]

16. Yu Y, Gao Y, Hu K, Blanchard PY, Noël JM, Nareshkumar T, Phani KL, Friedman G, Gogotsi Y, Mirkin MV. Electrochemistry and Electrocatalysis at Single Gold Nanoparticles Attached to Carbon Nanoelectrodes. ChemElectroChem. 2015; 2:58–63.

17. Xiao X, Bard AJ. Observing Single Nanoparticle Collisions at an Ultramicroelectrode by Electrocatalytic Amplification. J Am Chem Soc. 2007; 129:9610–9612. [PubMed: 17630740]

18. Fan FRF, Bard AJ. Observing Single Nanoparticle Collisions by Electrogenerated Chemiluminescence Amplification. Nano Lett. 2008; 8:1746–1749. [PubMed: 18491945]

19. Xiao X, Fan FRF, Zhou J, Bard AJ. Current Transients in Single Nanoparticle Collision Events. J Am Chem Soc. 2008; 130:16669–16677. [PubMed: 19554731]

20. Xiao X, Pan S, Jang JS, Fan FRF, Bard AJ. Single Nanoparticle Electrocatalysis: Effect of Monolayers on Particle and Electrode on Electron Transfer. J Phys Chem C. 2009; 113:14978–14982.

21. Kwon SJ, Fan FRF, Bard AJ. Observing Iridium Oxide (IrOx) Single Nanoparticle Collisions at Ultramicroelectrodes. J Am Chem Soc. 2010; 132:13165–13167. [PubMed: 20809574]

22. Quinn BM, van't Hof PG, Lemay SG. Time-Resolved Electrochemical Detection of Discrete Adsorption Events. J Am Chem Soc. 2004; 126:8360–8361. [PubMed: 15237976]

23. Jena BK, Percival SJ, Zhang B. Au Nanoelectrode by Electrochemical Deposition in a Nanopore. Anal Chem. 2010; 82:6737–6743. [PubMed: 20608658]

24. Park JH, Boika A, Park HS, Lee HC, Bard AJ. Single Collision Events of Conductive Nanoparticles Driven by Migration. J Phys Chem C. 2013; 117:6651–6657.

25. Kwon SJ, Bard AJ. Analysis of Diffusion-Controlled Stochastic Events of Iridium Oxide Single Nanoparticle Collisions by Scanning Electrochemical Microscopy. J Am Chem Soc. 2012; 134:7102–7108. [PubMed: 22452267]

26. Kim J, Kim BK, Cho SK, Bard AJ. Tunneling Ultramicroelectrode: Nanoelectrodes and Nanoparticle Collisions. J Am Chem Soc. 2014; 136:8173–8176. [PubMed: 24857267]

27. Boika A, Bard AJ. Time of First Arrival in Electrochemical Collision Experiments as a Measure of Ultralow Concentrations of Analytes in Solution. Anal Chem. 2015; 87:4341–4346. [PubMed: 25803279]

28. Alligrant TM, Anderson MJ, Dasari R, Stevenson KJ, Crooks RM. Single Nanoparticle Collisions at Microfluidic Microband Electrodes: The Effect of Electrode Material and Mass Transfer. Langmuir. 2014; 30:13462–13469. [PubMed: 25360826]

29. Robinson DA, Yoo JJ, Castañeda AD, Gu B, Dasari R, Crooks RM, Stevenson KJ. Increasing the Collision Rate of Particle Impact Electroanalysis with Magnetically Guided Pt-Decorated Iron Oxide Nanoparticles. ACS Nano. 2015; 9:7583–7595. [PubMed: 26168795]

30. Alligrant TM, Dasari R, Stevenson KJ, Crooks RM. Electrocatalytic Amplification of Single Nanoparticle Collisions Using DNA-Modified Surfaces. Langmuir. 2015; 31:11724–11733. [PubMed: 26457645]

31. Castañeda AD, Alligrant TM, Loussaert JA, Crooks RM. Electrocatalytic Amplification of Nanoparticle Collisions at Electrodes Modified with Polyelectrolyte Multilayer Films. Langmuir. 2015; 31:876–885. [PubMed: 25568965]

32. Kleijn SE, Lai SCS, Miller TS, Yanson AI, Koper MTM, Unwin PR. Landing and Catalytic Characterization of Individual Nanoparticles on Electrode Surfaces. J Am Chem Soc. 2012; 134:18558–18561. [PubMed: 23102515]

33. Kang M, Perry D, Kim YR, Colburn AW, Lazenby RA, Unwin PR. Time-Resolved Detection and Analysis of Single Nanoparticle Electrocatalytic Impacts. J Am Chem Soc. 2015; 137:10902–10905. [PubMed: 26264494]

34. Chen CH, Ravenhill ER, Momotenko D, Kim YR, Lai SCS, Unwin PR. Impact of Surface Chemistry on Nanoparticle-Electrode Interactions in the Electrochemical Detection of Nanoparticle Collisions. Langmuir. 2015; 31:11932–11942. [PubMed: 26448140]

35. Dasari R, Robinson DA, Stevenson KJ. Ultrasensitive Electroanalytical Tool for Detecting, Sizing, and Evaluating the Catalytic Activity of Platinum Nanoparticles. J Am Chem Soc. 2013; 135:570–573. [PubMed: 23270578]

36. Dasari R, Walther B, Robinson DA, Stevenson KJ. Influence of the Redox Indicator Reaction on Single-Nanoparticle Collisions at Mercury- and Bismuth-Modified Pt Ultramicroelectrodes. Langmuir. 2013; 29:15100–15106. [PubMed: 24188022]

37. Dasari R, Tai K, Robinson DA, Stevenson KJ. Electrochemical Monitoring of Single Nanoparticle Collisions at Mercury-Modified Platinum Ultramicroelectrodes. ACS Nano. 2014; 8:4539–4546. [PubMed: 24708257]

38. Robinson DA, Kondajji AM, Castañeda AD, Dasari R, Crooks RM, Stevenson KJ. Addressing Colloidal Stability for Unambiguous Electroanalysis of Single Nanoparticle Impacts. J Phys Chem Lett. 2016; 7:2512–2517. [PubMed: 27306603]

39. Zhou YG, Rees NV, Compton RG. Nanoparticle-Electrode Collision Processes: The Electroplating of Bulk Cadmium on Impacting Silver Nanoparticles. Chem Phys Lett. 2011; 511:183–186.

40. Zhou YG, Haddou B, Rees NV, Compton RG. The Charge Transfer Kinetics of the Oxidation of Silver and Nickel Nanoparticles via Particle-Electrode Impact Electrochemistry. Phys Chem Chem Phys. 2012; 14:14354–14357. [PubMed: 23007231]

41. Stuart EJE, Rees NV, Compton RG. Particle-Impact Voltammetry: The Reduction of Hydrogen Peroxide at Silver Nanoparticles Impacting a Carbon Electrode. Chem Phys Lett. 2012; 531:94–97.

42. Dickinson EJF, Rees NV, Compton RG. Nanoparticle-Electrode Collision Studies: Brownian Motion and the Timescale of Nanoparticle Oxidation. Chem Phys Lett. 2012; 528:44–48.

43. Kätelhõn E, Cheng W, Batchelor-McAuley C, Tschulik K, Compton RG. Nanoparticle-Impact Experiments Are Highly Sensitive to the Presence of Adsorbed Species on Electrode Surfaces. ChemElectroChem. 2014; 1:1057–1062.

44. Hao R, Fan Y, Zhang B. Electrochemical Detection of Nanoparticle Collision by Reduction of Silver Chloride. J Electrochem Soc. 2016; 163:H3145–H3151.

45. Guo Z, Percival SJ, Zhang B. Chemically Resolved Transient Collision Events of Single Electrocatalytic Nanoparticles. J Am Chem Soc. 2014; 136:8879–8882. [PubMed: 24909547]

46. Percival SJ, Zhang B. Fast-Scan Cyclic Voltammetry Allows Determination of Electron-Transfer Kinetic Constants in Single Nanoparticle Collision. J Phys Chem C. 2016; 120:20536–20546.

47. Li Y, Bergman D, Zhang B. Preparation and Electrochemical Response of 1–3 nm Pt Disk Electrodes. Anal Chem. 2009; 81:5496–5502. [PubMed: 19514727]

Biographies

Todd J. Anderson graduated from University of Washington with a B.S. degree in 2014. He subsequently joined Professor Bo Zhang's lab in the Department of Chemistry at UW. His research interests include the development of fluorescence-enabled electrochemical microscopy and massive electrochemical arrays for studying neuronal activity.

Bo Zhang is an Associate Professor of Chemistry at the University of Washington. His B.S. and M.S. degrees were obtained from Shandong University and Peking University, respectively. He worked with Henry White at the University of Utah and was awarded a Ph.D. in 2006. He joined the UW in 2008 after working in Andrew Ewing's lab. His research is focused on the use of nanoelectrodes and their massive arrays to understand single nanoparticles and neuronal communication.
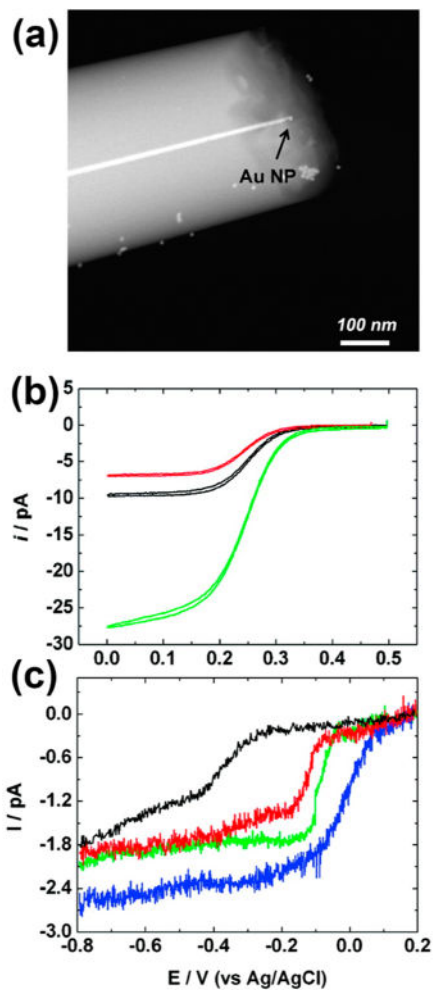
Figure 1.
(a) TEM image of a single Au nanoparticle immobilized on a Pt nanoelectrode. (b) CVs at 10 mV/s of a 9.0 nm bare Pt electrodes before (black), after APTMS-modification (red), and after modifying with a 24 nm Au particle (green) in 5.0 mM $K_3Fe(CN)_6$ and 0.2 M KCl. (c) CVs at 10 mV/s of a bare 7 nm Pt nanoelectrode (black), a 14 (red), an 18 (green), and a 24 nm Au SNPEs (blue) in an oxygen-saturated 0.10 M KOH solution. Reproduced with permission from ref 15. Copyright 2010 American Chemical Society.
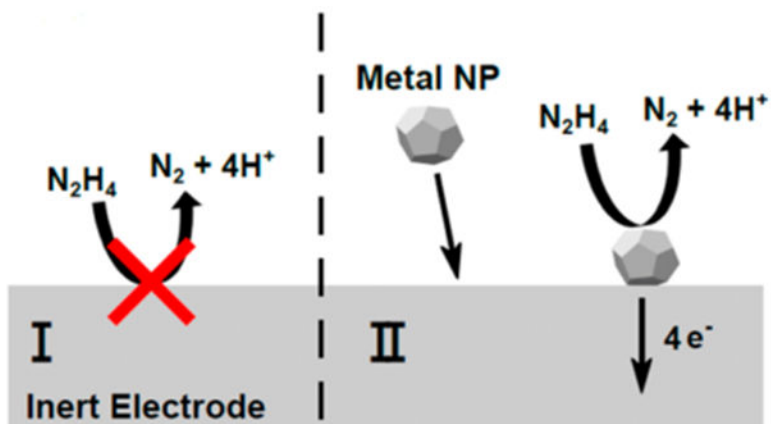
Figure 2.
General scheme for a single nanoparticle collision experiment. Reproduced with permission from ref 46. Copyright 2016 American Chemical Society.
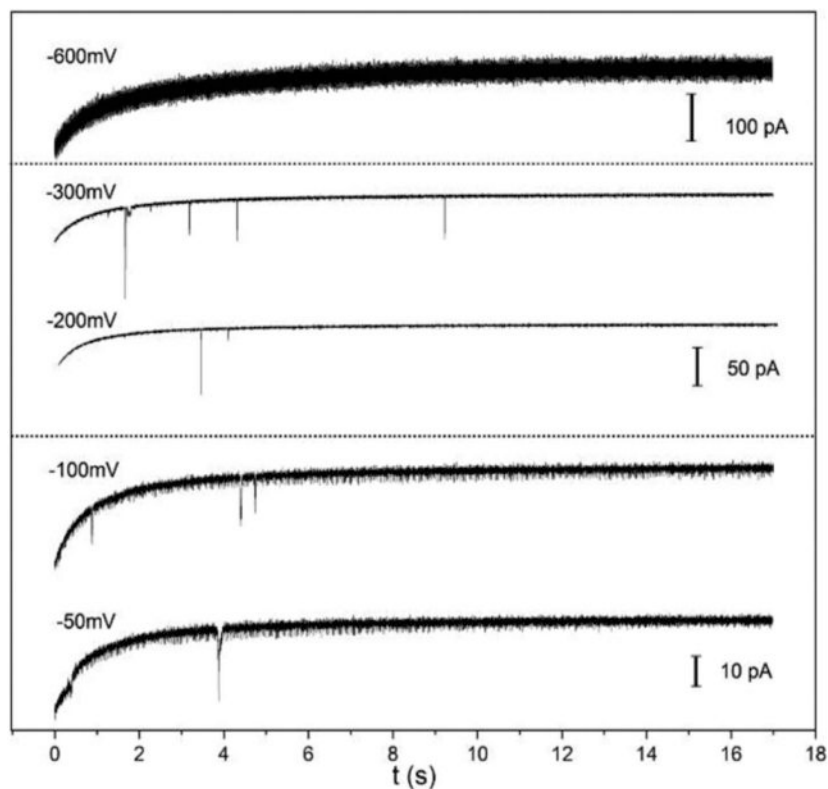
Figure 3.
Five amperometric traces of a 7 μm AgCl modified CFE showing detection of single collisional events of Ag nanoparticles at different potentials in 0.1 M KCl and 10 mM trisodium citrate containing 0.65 pM 80 nm Ag nanoparticles. Reproduced with permission from ref 44. Copyright 2016 Electrochemical Society.
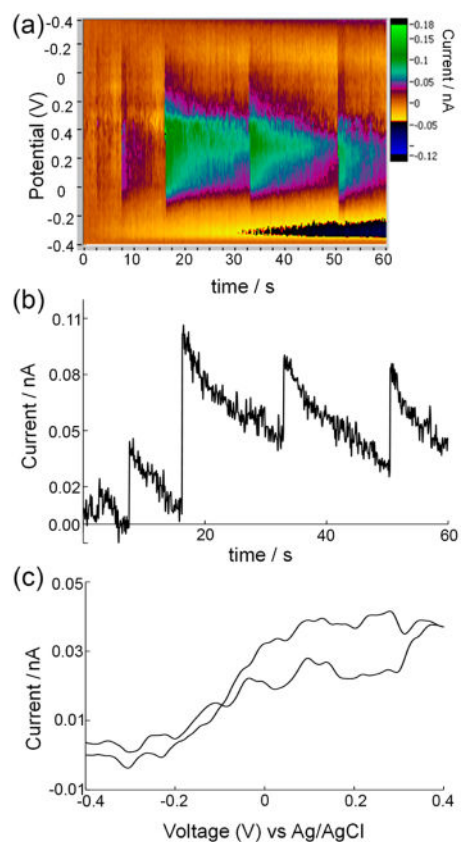
Figure 4.
Single collisional events of platinum nanoparticless on carbon. (a) A 60 s FSCV recording at
ν = 400 V/s showing detection of 5 Pt nanoparticles on a 5 μm CFE in a 15 mM hydrazine
solution. (b) Current–time trace taken from (a) at +0.1 V showing single-particle current
peaks similar to that recorded with amperometry. (c) Background-subtracted CV of a 4 nm
Pt particle recorded at 7.7 s in (a). Reproduced with permission from ref 45. Copyright 2014
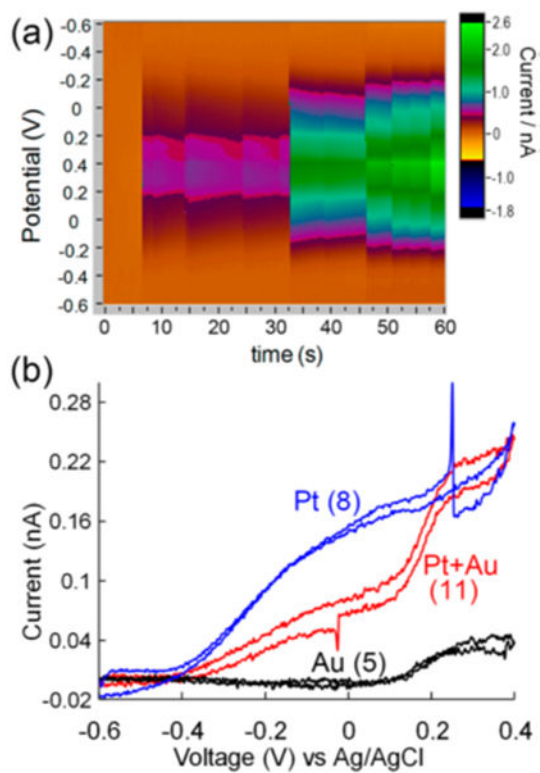American Chemical Society.

Figure 5.
Chemically resolving single nanoparticles. (a) A 60 s FSCV color plot showing detection of 11 single collision events on a 5 μm CFE in 15 mM hydrazine. (b) Single-particle CVs extracted from particles 8, 11, and 5, respectively. Reproduced with permission from ref 45. Copyright 2014 American Chemical Society.
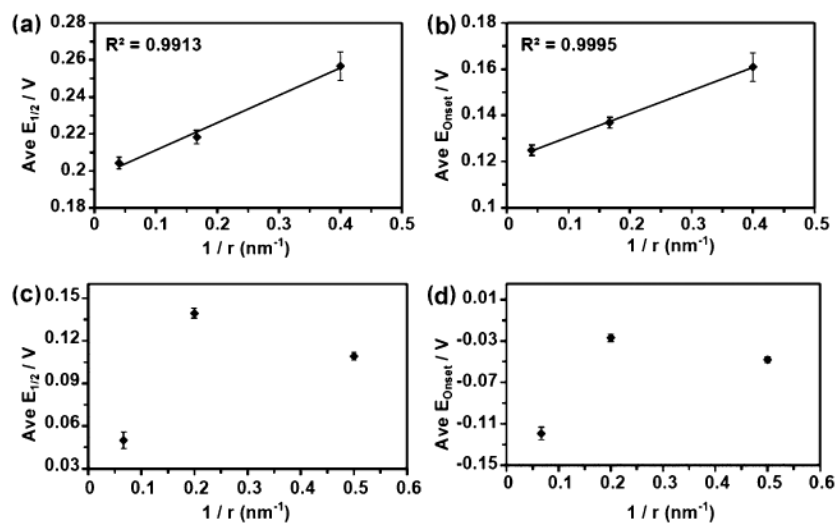
Figure 6.
Plots of the averaged $E_{1/2}$ and E_{onset} from all the mass transfer limited nanoparticle events vs the inverse of the TEM-determined radii. Panels (a) and (b) are from the gold particles and (c) and (d) are from the platinum particles. Error bars indicate standard error of the mean. Reproduced with permission ref 46. Copyright 2016 American Chemical Society.
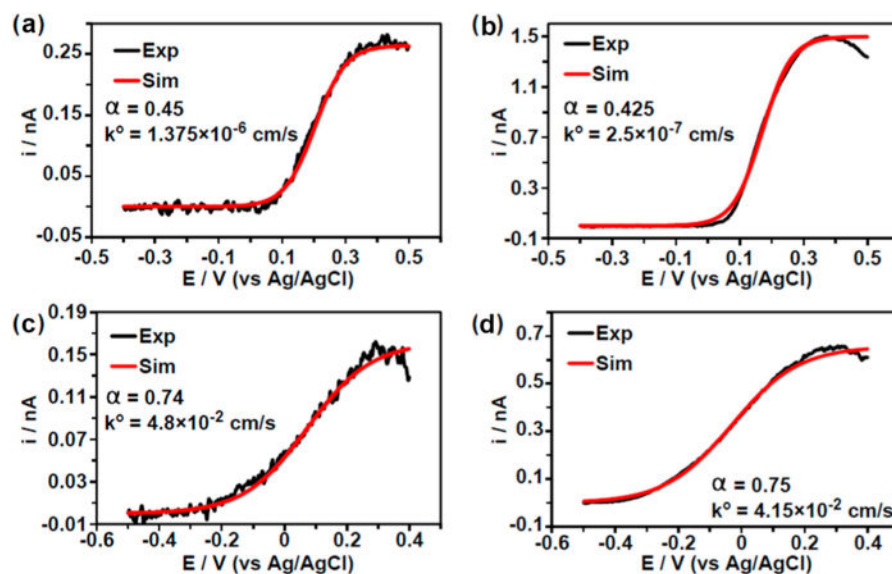
Figure 7.
Experimental CVs and their corresponding simulation from four example nanoparticles from the listed colloidal solutions: (a) 12 nm Au, (b) 50 nm Au, (c) 4 nm Pt, and (d) 30 nm Pt. Simulated CVs were obtained using the listed parameters. Only the forward scans are shown, and each experimental CV was taken at 25 V/s in 10 mM hydrazine containing 50 mM phosphate buffer (pH 7.4). Reproduced with permission ref 46. Copyright 2016 American Chemical Society.

Table 1

Averaged Values of the Different Nanoparticle "Batches" For the Charge Transfer Coefficient (a) Determined from Simulation and the Standard Heterogeneous Electron Transfer Rate Constant ($k°$)[a]

	a (simulation)	$k°$ (cm/s)
5 nm Au	0.540 ± 0.020	8.75 ± 3.7 (10^{-5})
12 nm Au	0.477 ± 0.015	9.64 ± 5.5 (10^{-6})
50 nm Au	0.501 ± 0.015	7.08 ± 4.2 (10^{-6})
4 nm Pt	0.742 ± 0.006	8.71 ± 2.0 (10^{-2})
10 nm Pt[b]	0.775 ± 0.003	7.66 ± 0.88 (10^{-2})
30 nm Pt	0.758 ± 0.007	4.23 ± 0.62 (10^{-2})

[a] Reproduced with permission ref 46. Copyright 2016 American Chemical Society.

[b] Cubic nanoparticles capped with polyacrylate.